Supporting Information

Defect-rich N/S-Co-doped Porous Hollow Carbon Nanospheres Derived from Fullerenes as Efficient Electrocatalysts for Oxygen Reduction Reaction and Zn-air batteries

Zhimin He [a], Peng Wei [a], Ting Xu [a], Jiantao Han [a], Xuejiao Gao [b,*] and Xing Lu [a,*]

[a] State Key Laboratory of Materials Processing and Die & Mould Technology, School of Materials Science and Engineering, Huazhong University of Science and Technology, 1037 Luoyu Road, Wuhan, 430074, P. R. China

[b] College of Chemistry and Chemical Engineering, Jiangxi Normal University, 99 Ziyang Road, Nanchang, Jiangxi, 330022, P. R. China

*Corresponding author: lux@hust.edu.cn (X. Lu)
gaoxj@jxnu.edu.cn (X.J. Gao)

1. Computational method

All geometries were fully optimized using B3LYP [1] density functional in conjunction with 6-31G(d, p) basis sets [2], which was applied in previous research on the ORR reactions on N/S dual doped graphene [3]. During optimization, SMD [4] solvation model was utilized to model the water environment. The harmonic frequency analysis was performed for each structure to identify whether the stationary point was a local minimum and to obtain the Gibbs free energy. NPA charge densities were calculated by natural population analysis. All the calculations were carried out using Gaussian 09 package [5].

In alkaline medium, the four-electron ORR mechanisms are defined as follows,

$$O_2 + 2H_2O + 4e^- \rightarrow {}^*O_2 + 2H_2O + 3e^- \quad \text{(S1)}$$

$${}^*O_2 + 2H_2O + 4e^- \rightarrow {}^*OOH + OH^- + H_2O + 3e^- \quad \text{(S2)}$$

$${}^*OOH + OH^- + H_2O + 3e^- \rightarrow {}^*O + 2OH^- + H_2O + 2e^- \quad \text{(S3)}$$

$${}^*O + 2OH^- + H_2O + 2e^- \rightarrow {}^*OH + 3OH^- + e^- \quad \text{(S4)}$$

$${}^*OH + 3OH^- + e^- \rightarrow 4OH^- \quad \text{(S5)}$$

$$\text{Overall}: O_2 + 2H_2O + 4e^- \rightarrow 4OH^- \quad \text{(S6)}$$

The first step of O_2 adsorption involves none electron transfer and thus the Eq. (1) and (2) are considered as a combined step.

Nørskov *et al.* presented that the free energy diagrams of ORR can be estimated by the following equation [6],

$$\Delta G = \Delta E + \Delta ZPE - T\Delta S + \Delta G_U + \Delta G_{pH} + \Delta G_{field} \quad \text{(S7)}$$

where ΔE, ΔZPE and ΔS were the total energy, zero-point energy and entropy difference of the products and reactants, respectively; T was the temperature which was considered as 298.15 K here; (ΔE + ΔZPE − TΔS) was the free Gibbs energy difference which can be obtained by DFT calculations directly; ΔG_U was defined as eU where U and e were the electrode potential with respect to standard hydrogen electrode and the charge transferred, respectively; $\Delta G_{pH} = 2.303\ k_B T \times pH$, where k_B was the Boltzmann

constant and the *p*H was 13 in the present work; ΔG_{field} was the free energy correction resulting from the electrochemical double layer and was neglected in the present study according to previous studies [6-9]. The free energy of O_2 was not calculated by DFT simulation but was obtained from the known free energy change of the reaction $O_2 + 2H_2 = 2H_2O$ under the standard condition, which was −4.92 eV. The free energy of OH^- was derived from the reaction $H^+ + OH^- = H_2O$.

According to Eq. (7), the free Gibbs energy differences for the four-electron reaction steps can be presented as follows,

$$\Delta G_1 = \Delta G_{*OOH} + eU_1 - 4.15 \quad \text{(S8)}$$

$$\Delta G_2 = \Delta G_{*O} - \Delta G_{*OOH} + eU_2 + 0.77 \quad \text{(S9)}$$

$$\Delta G_3 = \Delta G_{*OH} - \Delta G_{*O} + eU_3 + 0.77 \quad \text{(S10)}$$

$$\Delta G_4 = -\Delta G_{*OH} + eU_3 + 0.77 \quad \text{(S11)}$$

where the ΔG_{*OOH}, ΔG_{*O}, and ΔG_{*OH} were calculated according to the following reactions:

$$* + 2H_2O \rightarrow *OOH + 3/2\ H_2 \quad \text{(S12)}$$

$$* + H_2O \rightarrow *O + H_2 \quad \text{(S13)}$$

$$* + H_2O \rightarrow *OH + 1/2\ H_2 \quad \text{(S14)}$$

2. Supplementary Figures and Tables

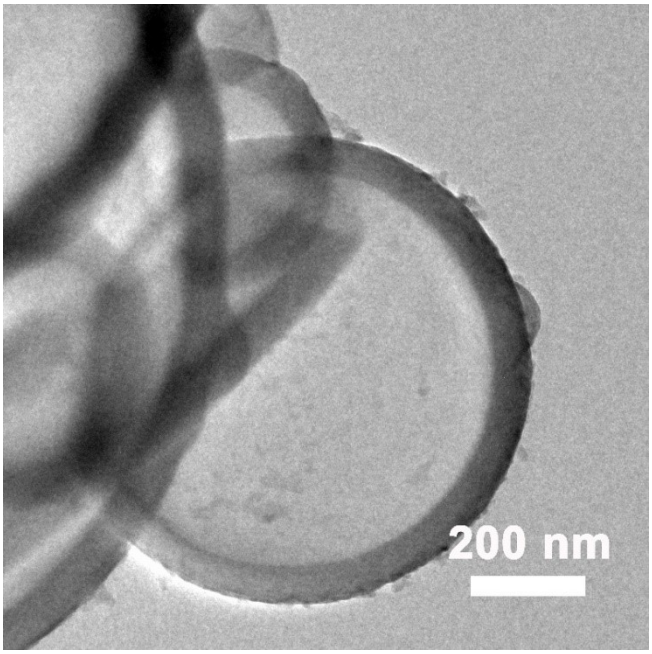

Figure S1 TEM image of FHCNSs.

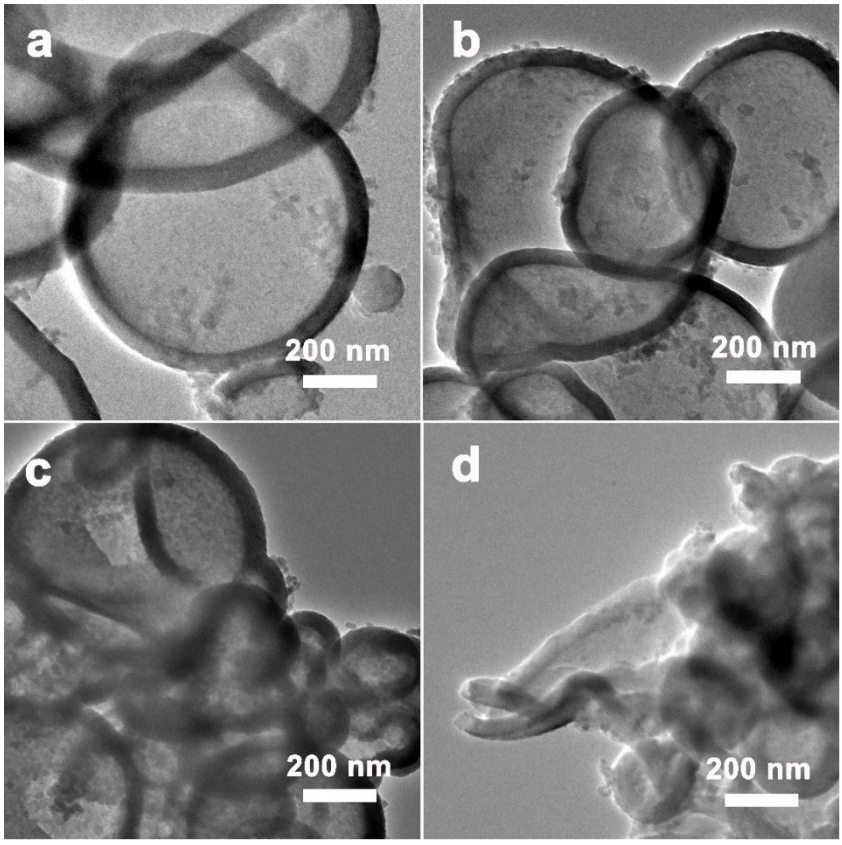

Figure S2 TEM images of (a) N-PHCNSs-700, (b) N-PHCNSs-800, (c) N-PHCNSs-900 and (d) N-PHCNSs-1000.

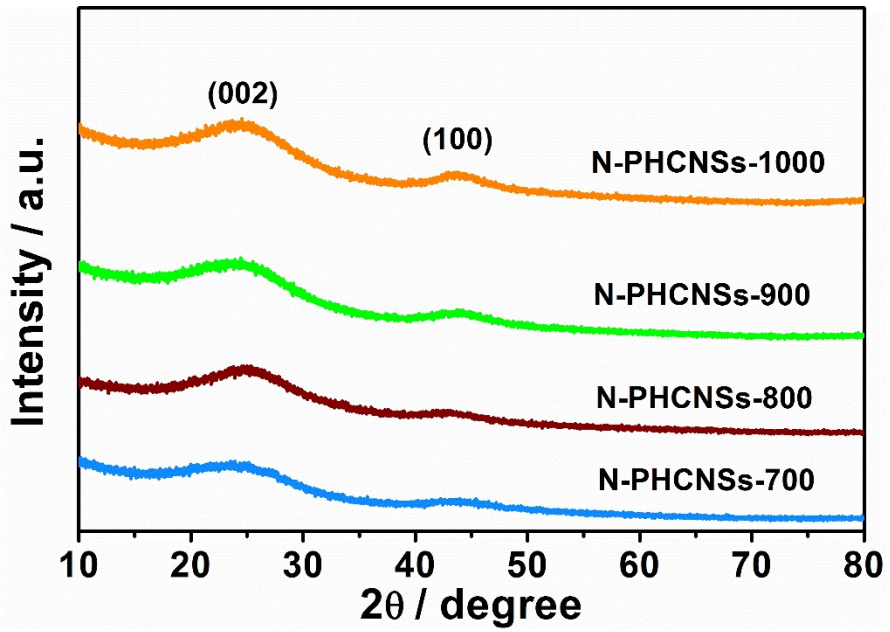

Figure S3 XRD patterns of N-PHCNSs-700, N-PHCNSs-800, N-PHCNSs-900 and N-PHCNSs-1000.

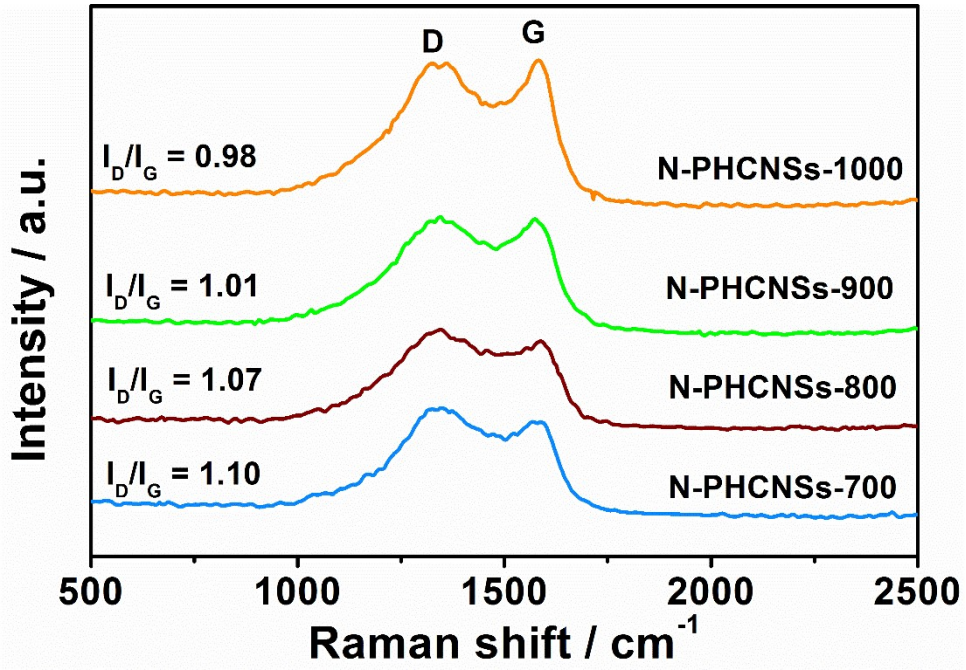

Figure S4 Raman spectra of N-PHCNSs-700, N-PHCNSs-800, N-PHCNSs-900 and N-PHCNSs-1000.

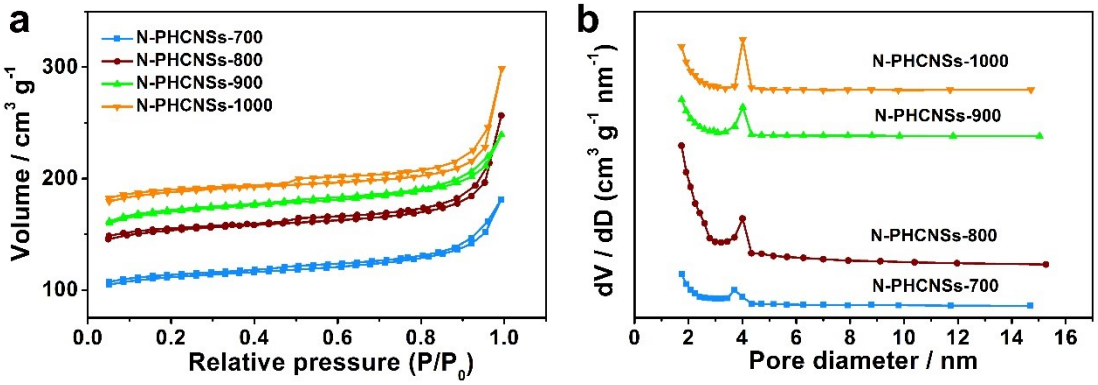

Figure S5 (a) N_2 adsorption/desorption isotherms and (b) the corresponding pore size distribution profiles of N-PHCNSs-700, N-PHCNSs-800, N-PHCNSs-900 and N-PHCNSs-1000.

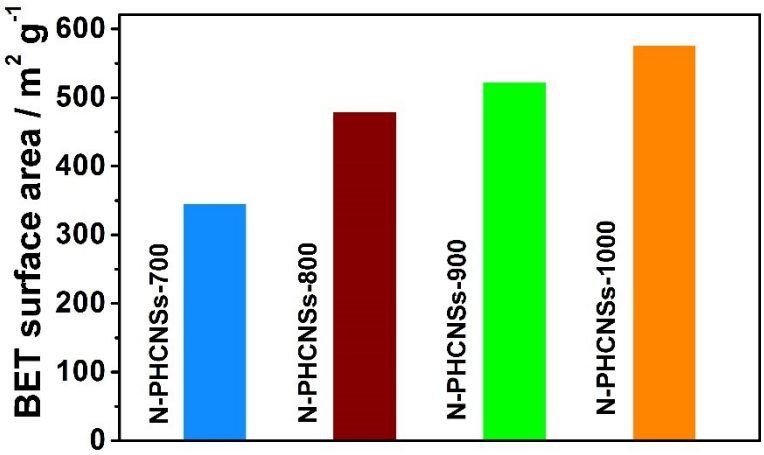

Figure S6 BET surface area survey of N-PHCNSs-700, N-PHCNSs-800, N-PHCNSs-900 and N-PHCNSs-1000, respectively.

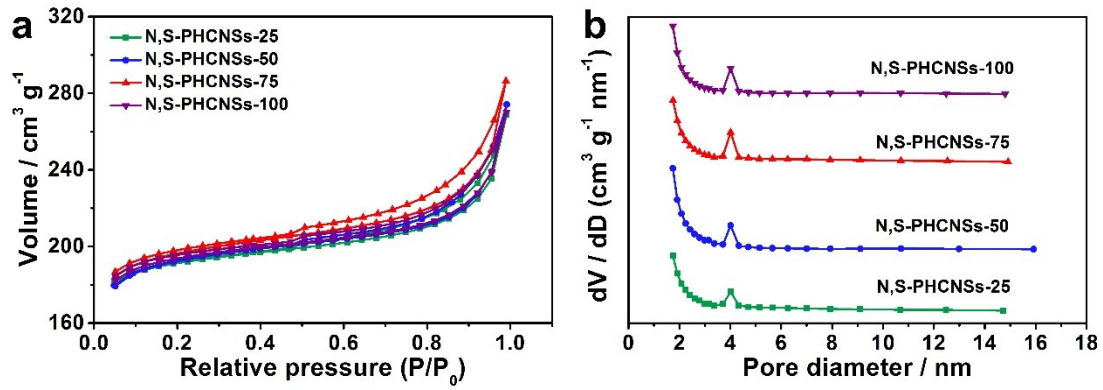

Figure S7 (a) N_2 adsorption/desorption isotherms and (b) the corresponding pore size distribution profiles of N,S-PHCNSs-25, N,S-PHCNSs-50, N,S-PHCNSs-75 and N,S-PHCNSs-100, respectively.

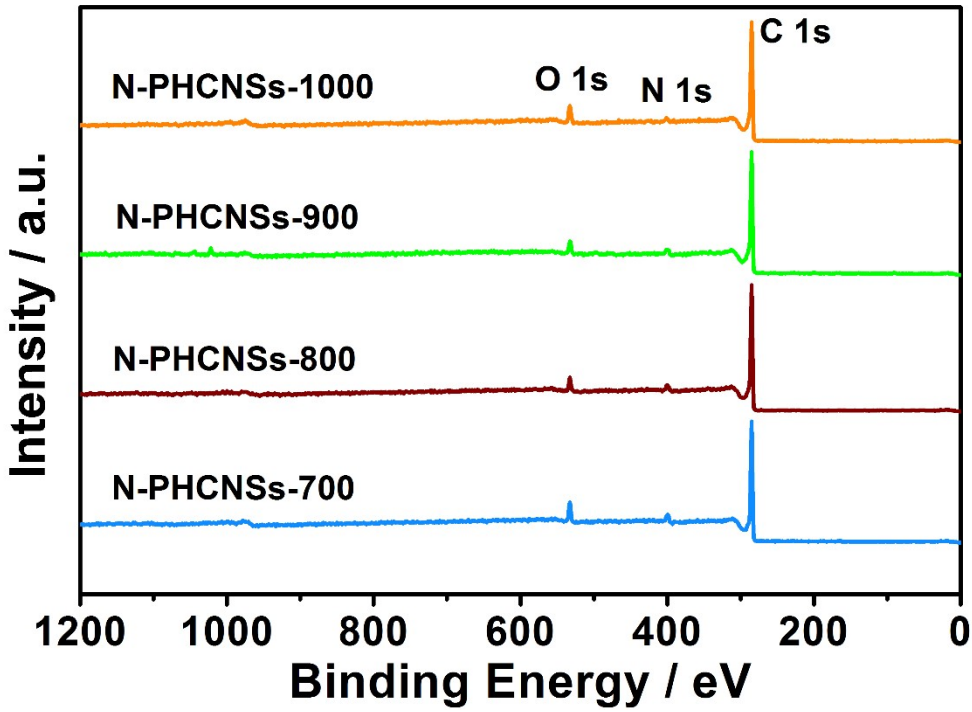

Figure S8 Full XPS spectra of N-PHCNSs-700, N-PHCNSs-800, N-PHCNSs-900 and N-PHCNSs-1000, respectively.

Table S1 Surface composition of N-PHCNSs catalysts under study.

Sample	C (at.%)	N (at.%)	O (at.%)
N-PHCNSs-700	86.64	6.30	7.06
N-PHCNSs-800	90.01	4.88	5.11
N-PHCNSs-900	91.77	2.90	5.33
N-PHCNSs-1000	92.16	1.65	6.19

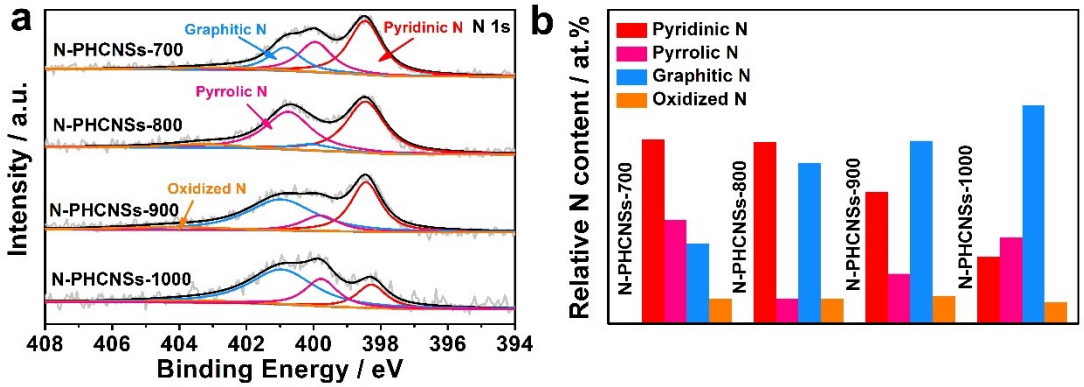

Figure S9 (a) High-resolution N 1s spectra and (b) the corresponding relative contents of various N species for N-PHCNSs-700, N-PHCNSs-800, N-PHCNSs-900 and N-PHCNSs-1000.

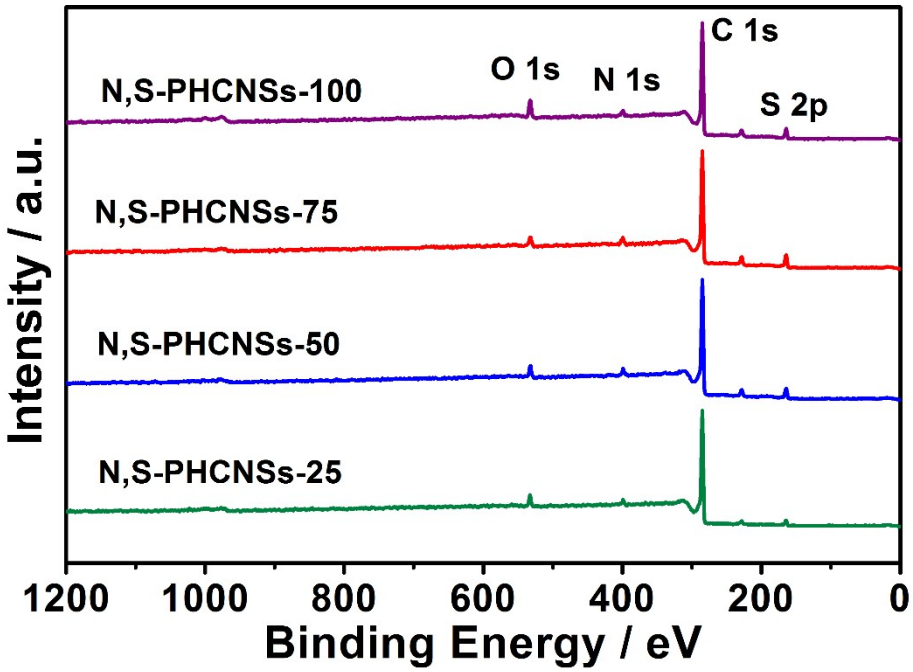

Figure S10 Full XPS spectra of N,S-PHCNSs-25, N,S-PHCNSs-50, N,S-PHCNSs-75 and N,S-PHCNSs-100, respectively.

Table S2 Surface composition of the N,S-PHCNSs catalysts under study.

Sample	C (at.%)	N (at.%)	S (at.%)	O (at.%)
N,S-PHCNSs-25	88.87	3.94	2.66	4.53
N,S-PHCNSs-50	88.23	2.96	4.25	4.56
N,S-PHCNSs-75	88.99	2.71	4.46	3.84
N,S-PHCNSs-100	89.47	1.29	5.58	3.66

Table S3 Element analysis of N,S-PHCNSs.

Sample	C (wt.%)	N (wt.%)	S (wt.%)	H (wt.%)
N,S-PHCNSs-25	82.33	4.02	5.82	1.33
N,S-PHCNSs-50	80.54	3.04	8.89	1.51
N,S-PHCNSs-75	81.02	2.88	9.29	1.19
N,S-PHCNSs-100	80.63	1.26	11.74	1.07

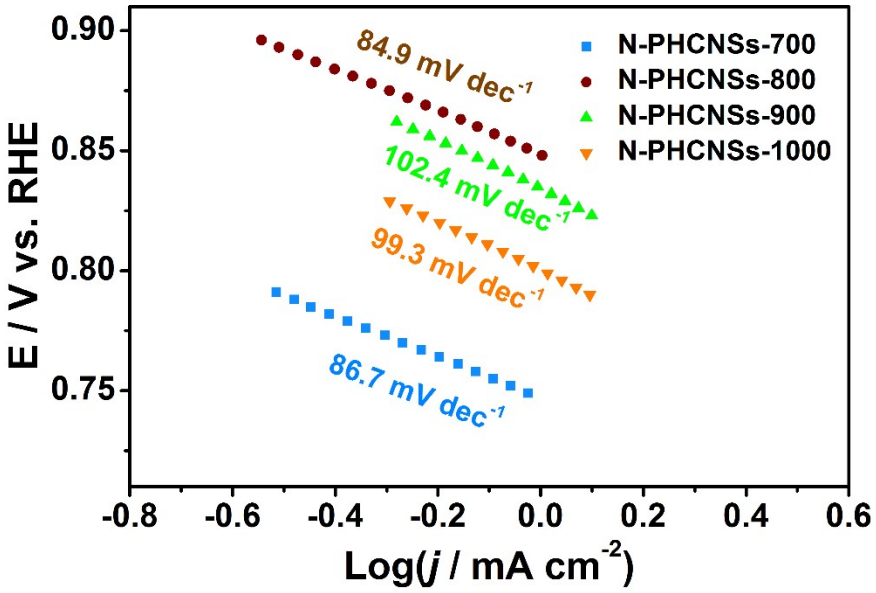

Figure S11 Tafel plots of N-PHCNSs-700, N-PHCNSs-800, N-PHCNSs-900 and N-PHCNSs-1000, respectively.

Table S4 The total contents (ppm) of metal elements in different samples detected by ICP-MS.

Sample	Fe	Co	Ni	Mn	Pt
Pristine C_{60} powder	0.3856	0.1784	0.2186	0.1881	/
FHCNSs	0.3903	0.1829	0.2578	0.2058	/
N,S-PHCNSs-75	0.4775	0.2523	0.3470	0.2826	/
N,S-PHCNSs-75-0	0.4240	0.2076	0.2757	0.2228	0.4454

Table S5 ORR activities of N-PHCNSs-800 and N,S-PHCNSs.

Catalysts	**E_0 (V)**	**E_0 (V)**	**E_0 (V)**
N-PHCNSs-800	0.917	0.779	5.58
N,S-PHCNSs-25	0.929	0.776	5.05
N,S-PHCNSs-50	0.932	0.811	5.42
N,S-PHCNSs-75	0.954	0.827	5.64
N,S-PHCNSs-100	0.934	0.803	5.09

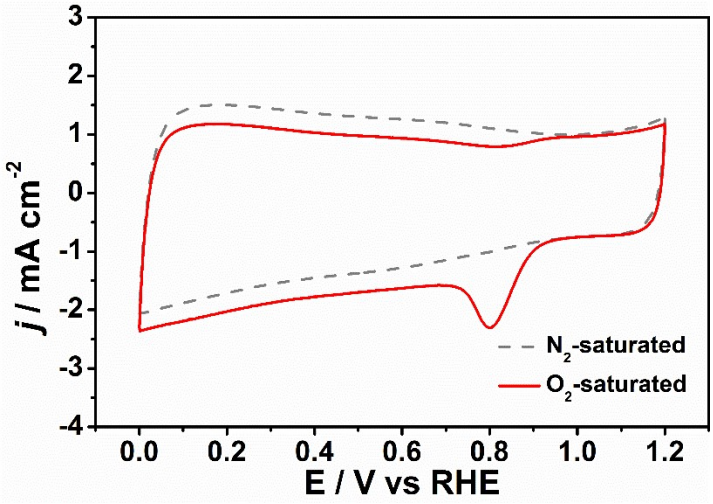

Figure S12 CV curves of N,S-PHCNSs-75 in O_2- and N_2-saturated 0.1 M KOH electrolyte. Scan rate: 50 mV s^{-1}.

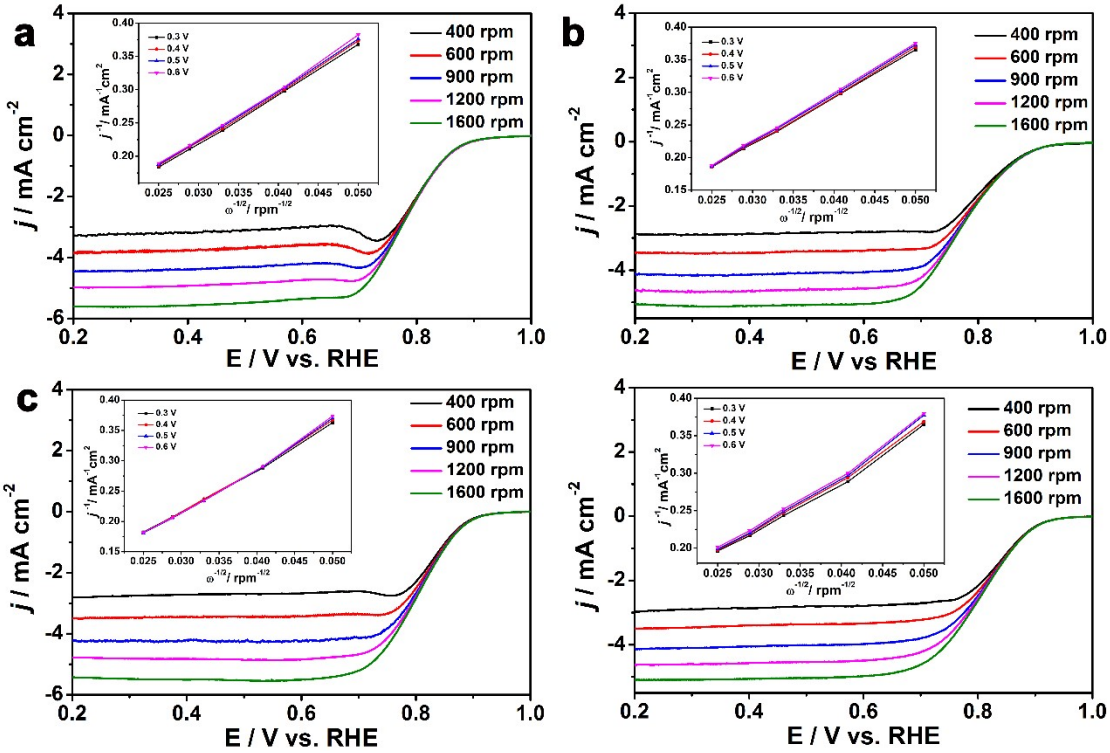

Figure S13 LSV curves with a scan rate of 10 mV s^{-1} at different rotation rates from 400 rpm to 1600 rpm and the corresponding K-L plots (insets) of (a) N-PHCNSs-800, (b) N,S-PHCNSs-25, (c) N,S-PHCNSs-50 and (d) N,S-PHCNSs-100, respectively.

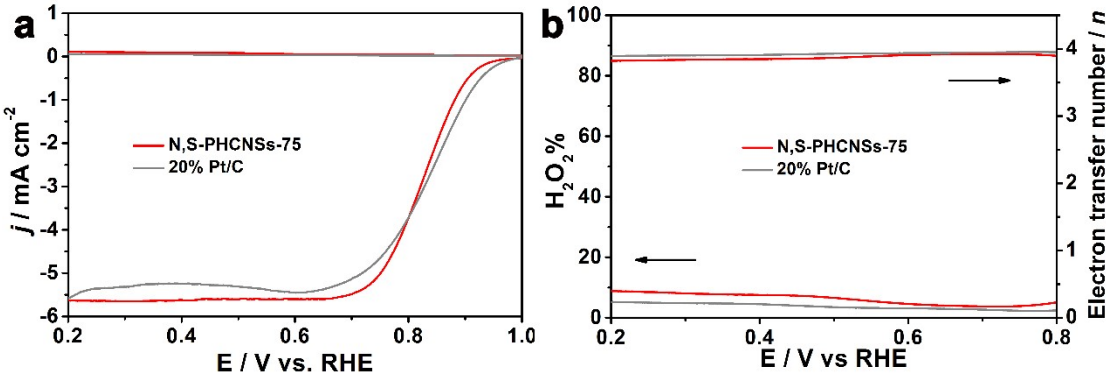

Figure S14 (a) RRDE tests of N,S-PHCNSs-75 and Pt/C catalysts. (b) The calculated H_2O_2 yield and calculated electron transfer number.

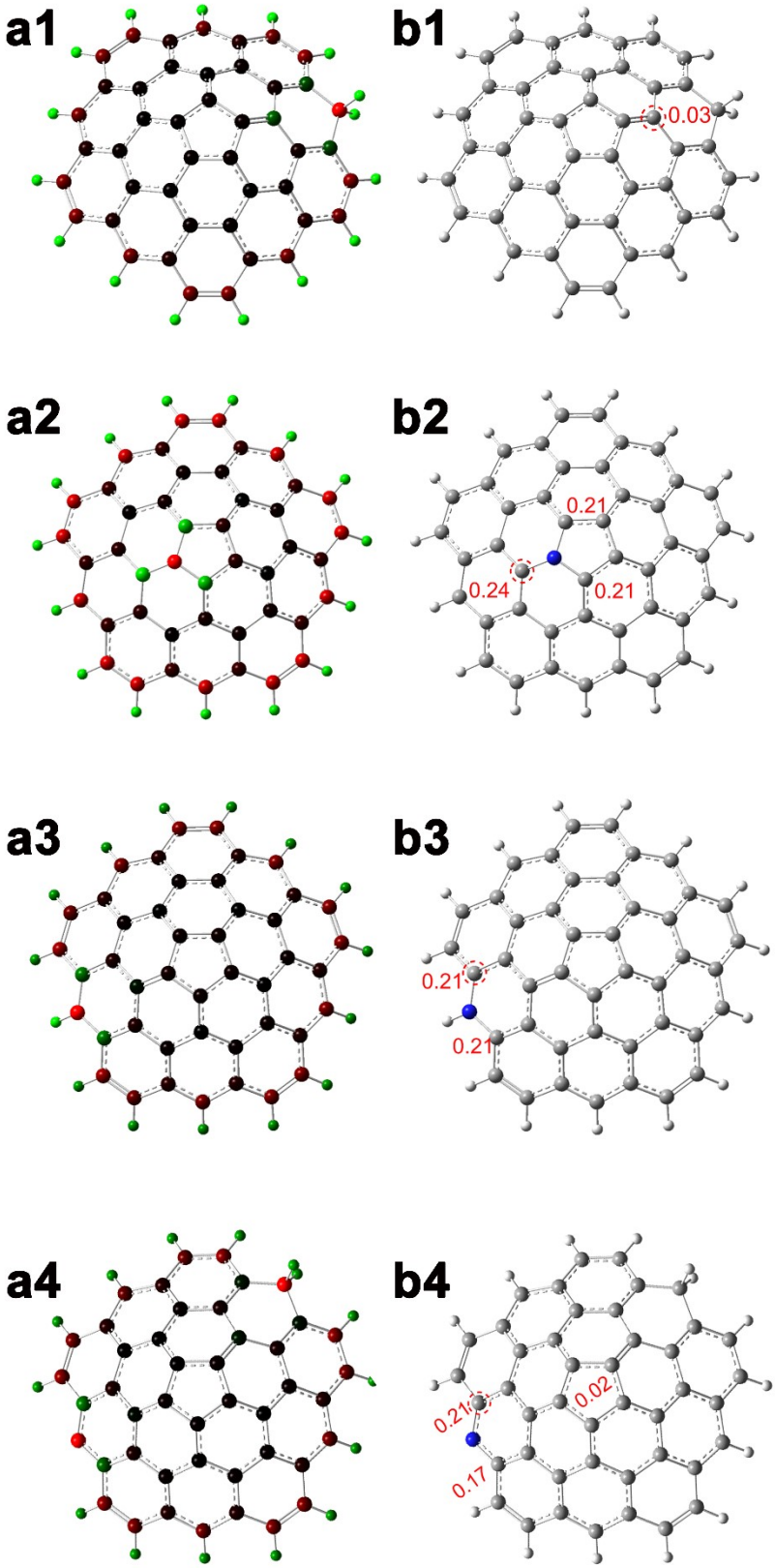

Figure S15 (a1-a4) Charge density and (b1-b4) the possible active sites of (1) PD, (2) gN-PD, (3) prN-PD and (4) pN-PD.

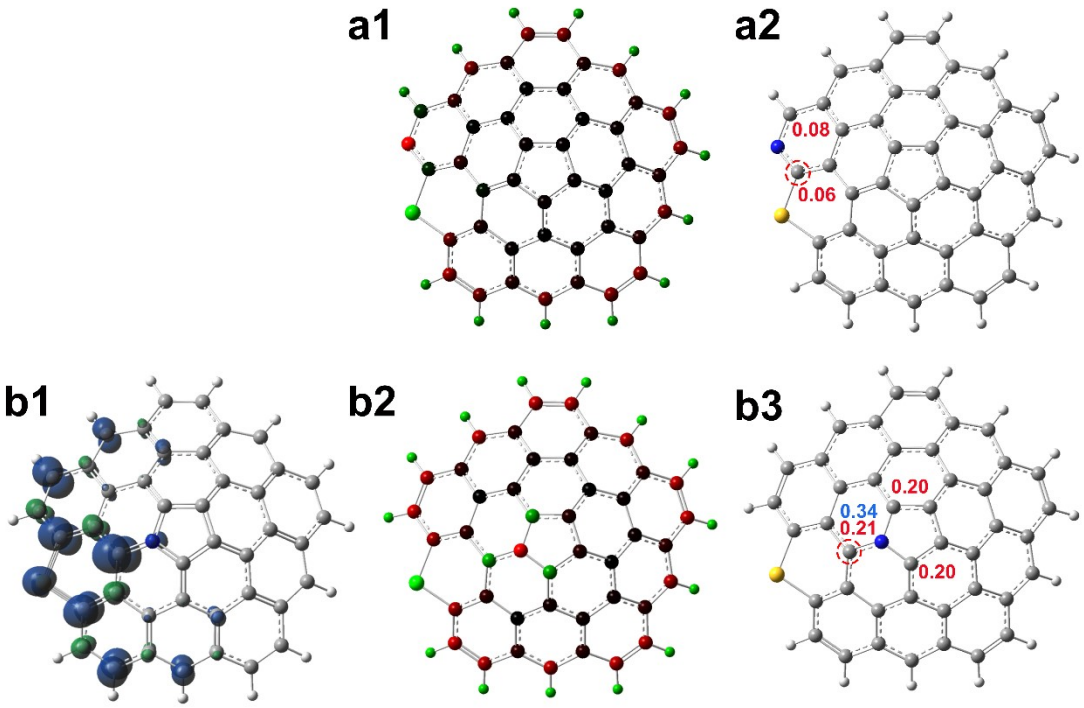

Figure S16 (a1) Charge density and (a2) the possible active sites of pNS-PD; (b1) spin density, (b2) charge density and (c3) the possible active sites of gNS-PD.

Table S6 Electrocatalytic ORR properties of different catalysts in 0.1 M KOH solution.*

Catalyst	Loading mass (mg cm^{-2})	E_0 (V)	$E_{1/2}$ (V)	J_L (mA cm^{-2})	Ref.
N,S-PHCNSs-75	**0.25**	**0.954**	**0.827**	**-5.64**	**This work**
N,S-PHCNSs-50	**0.25**	**0.932**	**0.811**	**-5.42**	**This work**
NSCNT-6	0.245	0.92	0.78	-	10
NS-CD@gf_a900	~0.28	0.93	0.75	-7.71	11
hSNCNC	0.12	0.898	0.793	-	12
PAC-5S	0.5	-	0.792	-6.19	13
CF-K-A	0.4	0.948	0.835	-	14
MNCNT-2	0.245	-	0.77	-3.90	15
LHNHPC	0.4	-	0.86	-4.4	16
NGM	~0.25	0.89	0.77	-6.41	17
NSPC-0.2-900	0.212	0.93	0.83	-5.8	18
N-hG6	0.25	0.91	0.833	-5.28	19
HHPC	~0.256	0.90	0.78	-5.34	20
NPCN-900	0.2	0.92	0.78	-5.50	21
NSG	0.25	0.835	0.785	-5.41	22
XWB-CMP-1000	0.306	0.866	0.786	-5.2	23

*For comparison, all the potential values above are *vs*. RHE. In 0.1 M KOH electrolyte (pH=13), E (*vs*. RHE) = E (*vs*. Ag/AgCl) + 0.197 V + 0.059 pH.

References

1. A. D. Becke, Density−functional thermochemistry. III. The role of exact

exchange, *J. Chem. Phy.*, 1993, **98**, 5648-5652.

2. G. A. Petersson and M. A. Al‐Laham, A complete basis set model chemistry. II. Open‐shell systems and the total energies of the first‐row atoms, *The J. Chem. Phy.*, 1991, **94**, 6081-6090.
3. J. Liang, Y. Jiao, M. Jaroniec and S. Z. Qiao, Sulfur and Nitrogen Dual-doped mesoporous graphene electrocatalyst for oxygen reduction with synergistically enhanced performance, *Angew. Chem. Int. Ed.*, 2012, **51**, 11496-11500.
4. A. V. Marenich, C. J. Cramer and D. G. Truhlar, Universal solvation model based on solute electron density and on a continuum model of the solvent defined by the bulk dielectric constant and atomic surface tensions, *J. Phy. Chem. B*, 2009, **113**, 6378-6396.
5. M. J. Frisch, G. W. Trucks, H. B. Schlegel, G. E. Scuseria, M. A. Robb, J. R. Cheeseman, G. Scalmani, V. Barone, B. Mennucci, G. A. Petersson, H. Nakatsuji, M. Caricato, X. Li, H. P. Hratchian, A. F. Izmaylov, J. Bloino, G. Zheng, J. L. Sonnenberg, M. Hada, M. Ehara, K. Toyota, R. Fukuda, J. Hasegawa, M. Ishida, T. Nakajima, Y. Honda, O. Kitao, H. Nakai, T. Vreven, J. A. Montgomery Jr., J. E. Peralta, F. Ogliaro, M. J. Bearpark, J. Heyd, E. N. Brothers, K. N. Kudin, V. N. Staroverov, R. Kobayashi, J. Normand, K. Raghavachari, A. P. Rendell, J. C. Burant, S. S. Iyengar, J. Tomasi, M. Cossi, N. Rega, N. J. Millam, M. Klene, J. E. Knox, J. B. Cross, V. Bakken, C. Adamo, J. Jaramillo, R. Gomperts, R. E. Stratmann, O. Yazyev, A. J. Austin, R. Cammi, C. Pomelli, J. W. Ochterski, R. L. Martin, K. Morokuma, V. G. Zakrzewski, G. A. Voth, P. Salvador, J. J. Dannenberg, S. Dapprich, A. D. Daniels, Ö. Farkas, J. B. Foresman, J. V. Ortiz, J. Cioslowski and D. J. Fox, Gaussian 09*Journal*, 2009.
6. J. K. Nørskov, J. Rossmeisl, A. Logadottir, L. Lindqvist, J. R. Kitchin, T. Bligaard and H. Jónsson, Origin of the overpotential for oxygen reduction at a fuel-cell cathode, *J. Phy. Chem. B*, 2004, **108**, 17886-17892.
7. W. Liang, J. Chen, Y. Liu and S. Chen, Density-functional-theory calculation analysis of active sites for four-electron reduction of O_2 on Fe/N-doped graphene, *ACS Catal.*, 2014, **4**, 4170-4177.
8. S. Zuluaga and S. Stolbov, Factors controlling the energetics of the oxygen reduction reaction on the Pd-Co electro-catalysts: Insight from first principles, *J. Chem. Phy.*, 2011, **135**, 134702.
9. Y. Wang, M. Jiao, W. Song and Z. Wu, Doped fullerene as a metal-free electrocatalyst for oxygen reduction reaction: A first-principles study, *Carbon*, 2017, **114**, 393-401.
10. Q. Yang, Z. Xiao, D. Kong, T. Zhang, X. Duan, S. Zhou, Y. Niu, Y. Shen, H. Sun, S. Wang and L. Zhi, New insight to the role of edges and heteroatoms in nanocarbons for oxygen reduction reaction, *Nano Energy*, 2019, **66**, 104096-104103.
11. J. Shin, J. Guo, T. Zhao and Z. Guo, Functionalized carbon dots on graphene as

outstanding non-metal bifunctional oxygen electrocatalyst, *Small*, 2019, **15**, 1900296-1900304.

12. H. Fan, Y. Wang, F. Gao, L. Yang, M. Liu, X. Du, P. Wang, L. Yang, Q. Wu, X. Wang and Z. Hu, Hierarchical sulfur and nitrogen co-doped carbon nanocages as efficient bifunctional oxygen electrocatalysts for rechargeable Zn-air battery, *J. Energy Chem.*, 2019, **34**, 64-71.
13. C. You, X. Jiang, L. Han, X. Wang, Q. Lin, Y. Hua, C. Wang, X. Liu and S. Liao, Uniform nitrogen and sulphur co-doped hollow carbon nanospheres as efficient metal-free electrocatalysts for oxygen reduction, *J. Mater. Chem. A*, 2017, **5**, 1742-1748.
14. J. Zhu, W. Li, S. Li, J. Zhang, H. Zhou, C. Zhang, J. Zhang and S. Mu, Defective N/S-codoped 3D cheese-like porous carbon nanomaterial toward efficient oxygen reduction and Zn-air batteries, *Small*, 2018, **14**, 1800563-1800571.
15. X. Ao, X. Xue, Z. Yang, Y. Yang and C. Wang, Nitrogen-doped braided-looking mesoporous carbonaceous nanotubes as an advanced oxygen reduction electrocatalyst, *Mater. Today Energy*, 2019, **12**, 62-69.
16. Y. Wang, H. Liu, K. Wang, S. Song and P. Tsiakaras, 3D interconnected hierarchically porous N-doped carbon with NH 3 activation for efficient oxygen reduction reaction, *Appl. Catal. B: Environ.*, 2017, **210**, 57-66.
17. C. Tang, H. F. Wang, X. Chen, B. Q. Li, T. Z. Hou, B. Zhang, Q. Zhang, M. M. Titirici and F. Wei, Topological defects in metal-free nanocarbon for oxygen electrocatalysis, *Adv. Mater.*, 2016, **28**, 6845-6851.
18. L. Wang, K. Liang, L. Deng and Y.-N. Liu, Protein hydrogel networks: A unique approach to heteroatom self-doped hierarchically porous carbon structures as an efficient ORR electrocatalyst in both basic and acidic conditions, *Appl. Catal. B: Environ.*, 2019, **246**, 89-99.
19. Y. Bian, H. Wang, J. Hu, B. Liu, D. Liu and L. Dai, Nitrogen-rich holey graphene for efficient oxygen reduction reaction, *Carbon*, 2020, **162**, 66-73.
20. X. Xiao, X. Li, Z. Wang, G. Yan, H. Guo, Q. Hu, L. Li, Y. Liu and J. Wang, Robust template-activator cooperated pyrolysis enabling hierarchically porous honeycombed defective carbon as highly-efficient metal-free bifunctional electrocatalyst for Zn-air batteries, *Appl. Catal. B: Environ.*, 2020, **265**, 118603-118610.
21. H. Jiang, Y. Wang, J. Hao, Y. Liu, W. Li and J. Li, N and P co-functionalized three-dimensional porous carbon networks as efficient metal-free electrocatalysts for oxygen reduction reaction, *Carbon*, 2017, **122**, 64-73.
22. I. S. Amiinu, J. Zhang, Z. Kou, X. Liu, O. K. Asare, H. Zhou, K. Cheng, H. Zhang, L. Mai, M. Pan and S. Mu, Self-organized 3D porous graphene dual-doped with biomass-sponsored nitrogen and sulfur for oxygen reduction and evolution, *ACS Appl. Mater. Interfaces*, 2016, **8**, 29408-29418.
23. S.-B. Ren, X.-L. Chen, P.-X. Li, D.-Y. Hu, H.-L. Liu, W. Chen, W.-B. Xie, Y. Chen, X.-L. Yang, D.-M. Han, G.-H. Ning and X.-H. Xia, Nitrogen and sulfur dual-doped carbon nanotube derived from a thiazolothiazole based conjugated microporous polymer as efficient metal-free electrocatalysts for oxygen

reduction reaction, *J. Power Sources*, 2020, **461**, 228145-228150.